Using the Observed Variations of the Start Date of the Rainy Season over Central America for Its Reliable Seasonal Outlook

JOANNA RODGERS,[a,b,c] VASUBANDHU MISRA,[a,b,c] AND C. B. JAYASANKAR[b,c]

[a] *Department of Earth, Ocean and Atmospheric Science, Florida State University, Tallahassee, Florida*
[b] *Center for Ocean-Atmospheric Prediction Studies, Florida State University, Tallahassee, Florida*
[c] *Florida Climate Institute, Florida State University, Tallahassee, Florida*

(Manuscript received 19 November 2023, in final form 30 May 2024, accepted 18 June 2024)

ABSTRACT: We introduce a simple method to define the start and the end of the rainiest part of the year as the first and the last day of the year when the daily rain rate is more or less than the annual mean climatological rain rate for a region or at a given grid point of the rainfall analysis, respectively. A novelty of this work is the adoption of a perturbation technique to generate a total of 1001 ensemble members to account for observational and analysis uncertainties. This allows for a probabilistic estimate of the start and retreat dates of the rainy season at the granularity of the Integrated Multi-satellitE Retrievals for Global Precipitation Measurement (IMERG), version 6, rainfall analysis over Central America. The seasonal cycle of the IMERG rainfall analysis is also found to verify with in situ observations in the region. Many large-scale climate drivers affect regional rainfall, often with complex interactions that affect the onset date, retreat date, and magnitude of the seasonal rainfall cycle, making it difficult to predict the length or total quantity of seasonal rainfall using climate drivers alone. Once an onset date is established, however, this metric alone can be more indicative of both the length and total seasonal rainfall anomaly than predicting how the climate drivers will interact to affect the quantity and duration of upcoming seasonal rainfall. The local relationships of the start date with seasonal length and rainfall anomaly are leveraged to produce effective seasonal outlooks of the rainy season for the region by just monitoring the start date variations.

SIGNIFICANCE STATEMENT: The start date and retreat date of the rainy season in Central America are defined every year, precisely to a specific date from our proposed definition of it. This is possible because the region exhibits a strong seasonality of the rainfall. As a result, the year-to-year (interannual) variation of the seasonal rainfall during the rainy season is also determined by the variations in the length of the season that are usually overlooked in fixed calendar seasons. We define the start or retreat date of the rainy season as the first or the last day of the year when the daily rain rate exceeds or falls below the average daily rainfall from 2001 to 2022, respectively. We also find that both start and retreat date variations independently influence the length and total seasonal rainfall of the rainy season. Consequently, these relationships are leveraged to provide an outlook of the forthcoming rainy season from the diagnosis of the variations of its onset date, which is shown to be an effective predictor with significant useful seasonal prediction skills.

KEYWORDS: Central America; Climate; Climate prediction; Forecast verification/skill; Seasonal forecasting; Interannual variability

1. Introduction

The isthmus of Central America comprising Panama, Costa Rica, Nicaragua, Honduras, El Salvador, Guatemala, and Belize has a distinct seasonal cycle of rainfall and a well-recognized monsoon system that is part of the unified view of the North and the South American Monsoon systems (Fig. 1; Vera et al. 2006). The seasonality of rainfall is vital for the region's economy (Wani et al. 2009; Alfaro 2014; Giraldo-Mendez et al. 2019; Loboguerrero et al. 2018; Stewart et al. 2022). However, the seasonal evolution of rainfall over Central America is rather heterogeneous given the region's complex geography (e.g., a narrow isthmus oriented northwest–southeast, surrounded by relatively warm oceans), topography, and location in the vicinity of the ITCZ. For example, the region's complex topography in the narrow isthmus and its interaction with the seasonally varying easterly trade winds give rise to a differing seasonal precipitation cycle between its Pacific and Caribbean slopes (Fig. 1; Magaña et al. 1999; Alfaro 2002; Taylor and Alfaro 2005; Amador et al. 2006). Furthermore, the north–south contrast in the rainy seasons from Panama to Belize is also distinct owing partly to the movement and extent of the ITCZ and its associated circulations and the strength and extent of the subtropical highs in the Pacific and the Atlantic Oceans. Additionally, the variability of the regional climate system forced by remote factors like ENSO, tropical North Atlantic SSTs (Durán-Quesada et al. 2017, 2020), and internal chaotic variations make anticipating or forecasting the seasonal hydroclimate over the region a challenging task (Alfaro et al. 2018; Kowal et al. 2023).

Supplemental information related to this paper is available at the Journals Online website: https://doi.org/10.1175/JCLI-D-23-0699.s1.

Corresponding author: Vasubandhu Misra, vmisra@fsu.edu

DOI: 10.1175/JCLI-D-23-0699.1

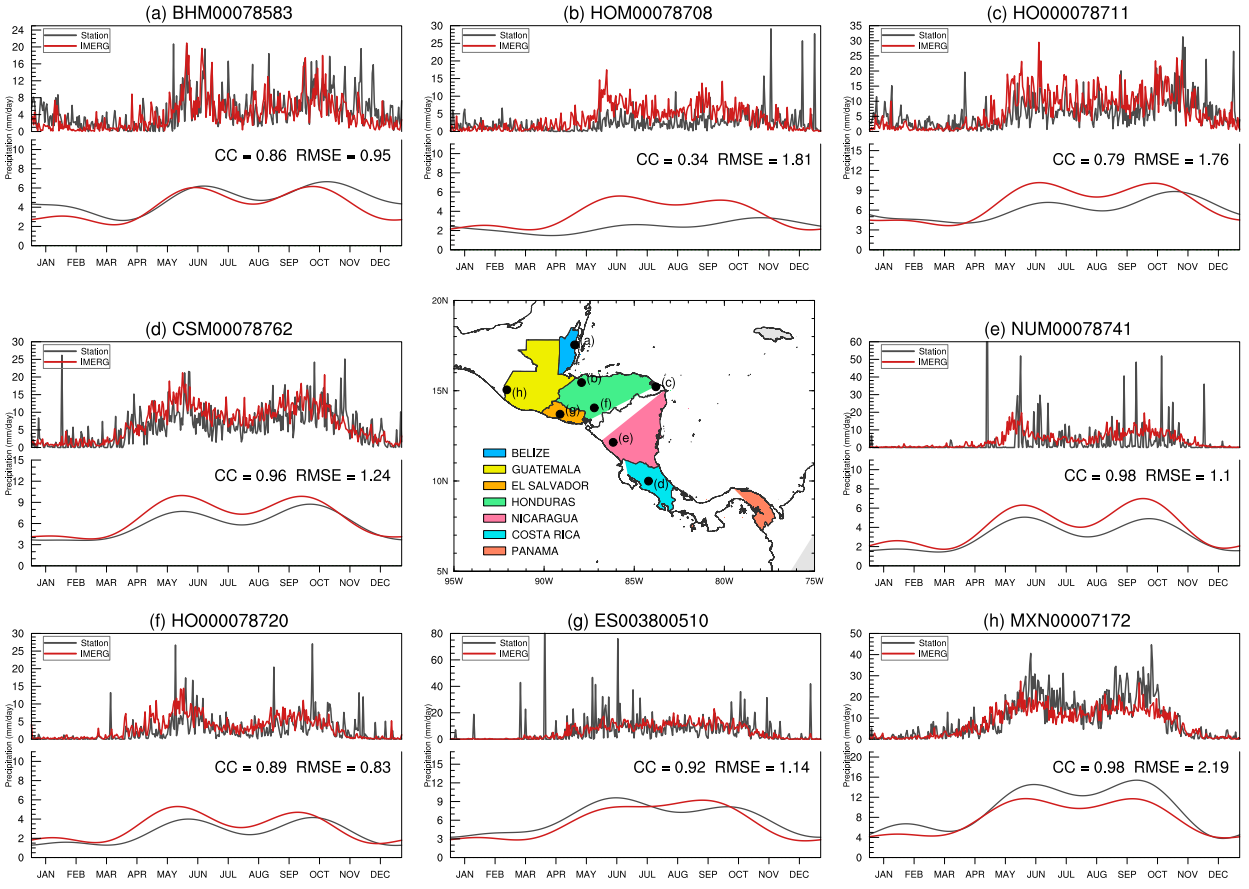

FIG. 1. The regional domain of Central America, which is the focus of this study, is at the center with eight selected NOAA's GHCN stations identified on the map. The time series of (top) daily climatology of rainfall (mm day^{-1}) and (bottom) its corresponding seasonal cycle (mm day^{-1}; isolated by harmonic analysis) for GHCN stations (black lines) (a) BHM00078583, (b) HOM00078708, (c) HO000078711, (d) CSM00078762, (e) NUM00078741, (f) HO000078720, (g) ES003800510, and (h) MXN00007172. The corresponding time series of the nearest grid point in the IMERG rainfall analysis is also plotted in all panels (red lines). The correlation coefficient (CC) and the RMSE (mm day^{-1}) of the seasonal cycle between the GHCN and the nearest IMERG rainfall analysis grid point time series of the daily climatology of the rainfall are also indicated in each panel.

Several earlier studies have examined the evolution of the rainy season and its predictability in the region (e.g., Gramzow and Henry 1972; Enfield and Alfaro 1999; Alfaro 2000; Nakaegawa et al. 2015; Martinez et al. 2019, 2020; Kowal et al. 2023). A number of these studies identify the start/retreat of the rainy season on daily or pentad rain-rate thresholds. For example, many studies use the start date of the rainy season as the first pentad of the year when it exceeds a threshold of 25 mm or more (e.g., Gramzow and Henry 1972; Enfield and Alfaro 1999). Enfield and Alfaro (1999) define the start date to be the first pentad when the rainfall $\geq$ 25 mm, with at least one of the two succeeding pentads exceeding 25 mm and the two pentads surrounding or following the latter at least have a trace amount of rainfall on average each day. While threshold-based definitions can be quite informative for sector-specific applications like for specific crop planting timing, such threshold-based methods are less widely applicable across different applications and large spatial scales. Furthermore, the threshold methodology could detect false start/retreat dates owing to random synoptic/mesoscale rain events that are not necessarily associated with the seasonal cycle (Flatau et al. 2003). Additionally, the predetermined threshold could potentially change in a changing climate (Hidalgo et al. 2013). Martinez et al. (2019, 2020) use pentads to reduce the noise in the daily or subdaily rainfall and define the rainy season between the 17th and the 67th pentad to account for the temporal variations of the season across Central America. Here, the disadvantage is that the 5-day averaging of the pentad reduces the temporal resolution of the rainfall data when there is a growing repository of remotely sensed data at subdaily intervals (Zambrano-Bigiarini et al. 2017).

In this paper, we offer a simple but effective way to define the start and the retreat of the rainy season across Central America at the native resolution of the observational dataset of rainfall (in our case, it is at 10-km grid). The proposed methodology has been successfully implemented in other regions like India (Bhardwaj and Misra 2019), northern Australia (Uehling and Misra 2020; Misra et al. 2023), and Florida (Misra et al. 2022). This method identifies the "rainiest" period of the

year objectively as the first and the last day of the year when the daily rain rate is greater than the corresponding annual mean climatological daily rain rate. As a result, the methodology is still able to identify a rainy season even in regions of Central America along the Caribbean coast that rain for most of the year and barely display a "dry" season (e.g., Alfaro 2002; Hidalgo et al. 2017). This method also differs from earlier studies that split the rainy season into an early rainy period (May–July) and a late rainy period (August–October) (e.g., Alfaro et al. 2018; Kowal et al. 2023). This splitting of the rainy season is roughly on either side of the mid-summer drought (MSD). Magaña et al. (1999) define the bimodal distribution of rainfall over southern Mexico and Central America with peaks in June and September–October and a relative minimum in July and August as MSD. In this study, we span the entire rainy season including the MSD as our methodology is unable to make the distinction between the two periods. Furthermore, assessing and providing the seasonal outlook for the entire rainy season allows for more lead time in planning to mitigate or adapt to the impacts of the anomalous season and complements the other efforts to assess the early and late rain periods.

A localized approximation of the start date could be a simpler option to estimate key wet season characteristics compared to relying on an assessment of the complex interactions between known rainfall drivers. Unlike some of the other expansive monsoonal regions (e.g., the Asian monsoon and the Australian monsoon), the Central American region as mentioned earlier has a complex evolution of the wet season that evolves zonally and meridionally giving rise to sharp spatial gradients of rainfall (Hidalgo et al. 2015). The large-scale teleconnections with neighboring ocean basins are also complicated (Durán-Quesada et al. 2020). For example, the role of ENSO and ITCZ variability in the interannual variability of Central American rainfall is not uniform. ENSO variations affect the trade winds, the Caribbean low-level jet, and the meridional location of ITCZ, which in turn impact the moisture transport and consequently modulate rainfall over the Central American isthmus differently between the Pacific and the Caribbean coasts (Amador et al. 2016a,b; Durán-Quesada et al. 2020). Several studies suggest that with a cold or warm phase of ENSO, there is an associated increase or decrease of rainfall along the Pacific coast of Central America, respectively (Dai and Wigley 2000; Giannini et al. 2000; Cid-Serrano et al. 2015; Hidalgo et al. 2017; Maldonado et al. 2016, 2018; Sánchez-Murillo et al. 2016). This teleconnection is, however, impacted by the SST gradient between the tropical Pacific and tropical North Atlantic Oceans (Enfield and Alfaro 1999). Waylen et al. (1996) suggest that ENSO teleconnections over Central America are strongly constrained by the orographic effects on either side of the Central Cordillera giving rise to local, discrete teleconnection patterns. In this study, we use a perturbed ensemble of daily rainfall data with a simple but effective definition of the rainy season (following Misra et al. 2023) to provide a more granular view of the start and retreat of the Central American rainy season. We leverage this more localized analysis to examine the seasonal predictability of the regional rainfall. In the following section, we describe the datasets and methodology followed by a discussion of the results in section 3. The concluding remarks are provided in section 4.

2. Datasets and methodology

The daily rainfall data were obtained from the Integrated Multi-satellitE Retrievals for Global Precipitation Measurement (IMERG), version 6 (Huffman et al. 2019), as the primary dataset. The IMERG rainfall analysis was made available at 0.1° grid spacing (~10 km) at half-hourly temporal resolution from June 2000 to the present. The IMERG data also include the rainfall analysis that is labeled early, late, and final run products which have a latency of ~4 h, 12 h, and 3.5 months, respectively. The latency of these products is dictated by the time taken for data ingestion, preprocessing the use of the kinds of satellite radiances collected by the Global Precipitation Measurement (GPM), the adopted analysis technique, and the availability and use of the atmospheric reanalysis products for the release of the final gridded rainfall product (Huffman et al. 2019). Since the methodology introduced in this study to diagnose the evolution of the rainy season is also being adapted for real-time monitoring of the season, we chose to use the 12-h latency (late) product of IMERG. A 12-h latency will not affect the real-time application and would also take advantage of the additional preprocessing done relative to the 4-h latency product. For this study, we have computed the daily sum of 12-h latency IMERG product from its half-hourly interval. This IMERG dataset is also verified for its seasonal cycle for eight stations from NOAA's Global Historical Climatology Network (GHCN; Menne et al. 2012), shown in Fig. 1. We isolated eight stations (as indicated in Fig. 1) for this study that covered as wide an area of Central America as possible and had the longest record of daily rainfall data in the region with the least missing data (with at least 10 years available for each day of the year) to develop a robust climatology. As a result of this latter criterion, no GHCN stations were identified in Panama. To compare the IMERG rainfall analysis data to these eight stations, we choose the nearest grid point. The seasonal cycle from the time series as indicated in Figs. 1a–f is isolated by summing the first four harmonics from the daily precipitation climatology (Murakami et al. 1986; Jayasankar et al. 2015).

The methodology adopted in this study to diagnose the start and retreat of the rainy season has been widely used for many of the tropical regions that show strong seasonality of rainfall (Liebmann and Marengo 2001; Misra and DiNapoli 2014; Dunning et al. 2016; Bombardi et al. 2019; Uehling and Misra 2020). Essentially, this methodology diagnoses the start and the retreat dates of the rainy season as the first and the last day of the year when the daily rain rate is more than the corresponding average daily rainfall from 2001 to 2022, respectively. This is achieved by isolating the inflection points on the daily cumulative anomaly curve of the rainfall (Fig. S1 in the online supplemental material). The cumulative anomaly curve of the daily rainfall for the ith day of the mth year at the jth grid point [$C_m(i, j)$] is given by

$$C_m(i, j) = \sum_{n=1}^{i} [p_m(n, j) - \overline{\overline{p}}(j)], \quad (1)$$

where p_m (n, j) is the precipitation of the nth day in the mth year at the jth grid point, $\overline{\overline{p}}(j) \equiv$ annual mean climatological rain rate of the jth grid point $= (1/MN)\sum_{m=1}^{M}\sum_{n=1}^{N} p_m(n, j)$, M is the total number of years, and N is the total number of days in each year.

This methodology is effective only where there is a strong seasonality of rainfall (Fig. S2). It should be noted that for this study, the annual mean climatological rain rate at each grid point was computed over the period of 2001–22. If the daily rainfall data are averaged over a large area [e.g., over India in Noska and Misra (2016) or over Northern Australia in Uehling and Misra (2020)], then the chances of getting false start and retreat dates are highly unlikely, as spatial averaging reduces noise in the time series. However, in this study, where the methodology is adopted at every grid point of IMERG rainfall analysis which is at 10-km grid spacing, there is a greater likelihood of obtaining false start and retreat dates of the rainy season. To preclude diagnosis of false start and retreat dates from the excessive bearing of isolated synoptic or subsynoptic rain-bearing systems, which may be unconnected to the large-scale seasonality of the rainfall in the region, we introduce a perturbation technique following Misra et al. (2023). In a region like Central America, this may be particularly relevant where mesoscale convective systems are abundant (Liu and Zipser 2013, 2015). Additionally, the ensemble of start and retreat dates obtained from the perturbed time series also reflects on the uncertainty of observations and analysis techniques of the rainfall data. The uncertainty of the analysis techniques refers to the production of discretized rainfall data on regular (10 km) grids from converting the pixel data of radiance of microwave sensors obtained from multiple satellite platforms combined with Ku band radar sensors, adjusted with rainfall estimates from several other sources (Huffman et al. 2019).

Following Misra et al. (2023), the perturbations to the time series are generated by shuffling the original daily time series of rainfall on the time scale of 7 days (representing synoptic scales) with rain rates of every day being replaced by rain rates occurring within the sequence of ±3 days of the chosen date. We generate 1000 such perturbed time series per year per grid point. The spread and the ensemble mean of the 1001 (=1000 perturbations + the original) time series for a sample year and for a sample grid point over Nicaragua are shown in Fig. S3. The start and retreat of the rainy season is computed at every grid point of the IMERG product (at its 0.1° grid resolution) for all 1001 ensemble members across Central America for the period of the dataset (2001–22). Therefore, a random rain event that exceeds the annual mean climatological daily rain rate and is unconnected with the annual cycle either average out in the ensemble mean or will yield, for example, an anomalous start date with very low probability.

Our methodology ignores the MSD phenomenon in the region, which gives rise to the bimodal peak of rainfall in the region (Fig. S2). Although significant importance is attached separately to the variations of the primary peak (May–June) and secondary maximum (September–October) of rainfall (Magaña et al. 1999; Alfaro et al. 2018), there is still significant rainfall during the July–August period of the MSD in many locations (>5 mm day^{-1}; Fig. S2) while some locations will receive almost no rainfall in some years.

Some of the following indices are used in the study to gauge the remote influence on the variations of the Central American hydroclimate:

1) **ENSO index**: The seasonally averaged SST over the Niño-3.4 region.
2) **Interbasin index**: It is the seasonal mean SST difference between the tropical Atlantic region (80°–40°W and 10°–25°N) and tropical Pacific region (160°E–160°W and 0°–10°N) following Kim et al. (2020).
3) **Atlantic warm pool index**: The area enclosed by the 28.5°C SST in the tropical Atlantic following Wang and Enfield (2001) and is averaged from the date of onset of the warm pool to its demise following Misra et al. (2014). The climatological onset and demise date of the warm pool is 20 June and 2 November, respectively (Misra et al. 2014).
4) **Tropical northeast Pacific warm pool index**: The area enclosed by the 28.5°C SST in the tropical northeast Pacific following Wang and Enfield (2001) and is averaged from the date of onset of the warm pool to its demise following Misra et al. (2016). The climatological onset and demise date of the warm pool is 22 March and 16 August, respectively (Misra et al. 2016).
5) **Tropical North Atlantic index**: The area averaged SST from 60° to 20°W and 10° to 20°N following Misra (2006).

We have also applied the field significance test on the teleconnection patterns following Livezey and Chen (1983). We used 500 Monte Carlo simulations to assess field significance at the 95% confidence interval.

Finally, the verification of the seasonal outlook of the rainy season presented in section 3d is done using the area under the relative operating characteristic curve (AROC), which measures the probabilistic skill of the outlook, obtained from the 1001-member ensemble of the adopted methodology. The seasonal outlook at a given grid point in the domain is considered useful if its corresponding AROC is ≥0.5 (Narotsky and Misra 2022; Mason and Graham 1999). The AROC has become part of the World Meteorological Organization (WMO) standardized verification system for assessing the quality of forecasts and is widely used to assess the quality of probabilistic forecast systems (Stanski et al. 1989; WMO 2000; Mason and Graham 2002).

3. Results

a. *Verification*

The climatological seasonal cycle of rainfall for all eight GHCN stations is shown in Fig. 1. In this figure, we have also overlaid the corresponding IMERG rainfall from the closest grid point to the station for verification. It is to be noted that the fidelity of the seasonal cycle of the IMERG data is important in identifying the start/retreat of the rainy season. The correlations of the seasonal cycle between the two time series are over 0.75 for seven of the eight stations. Similarly, the

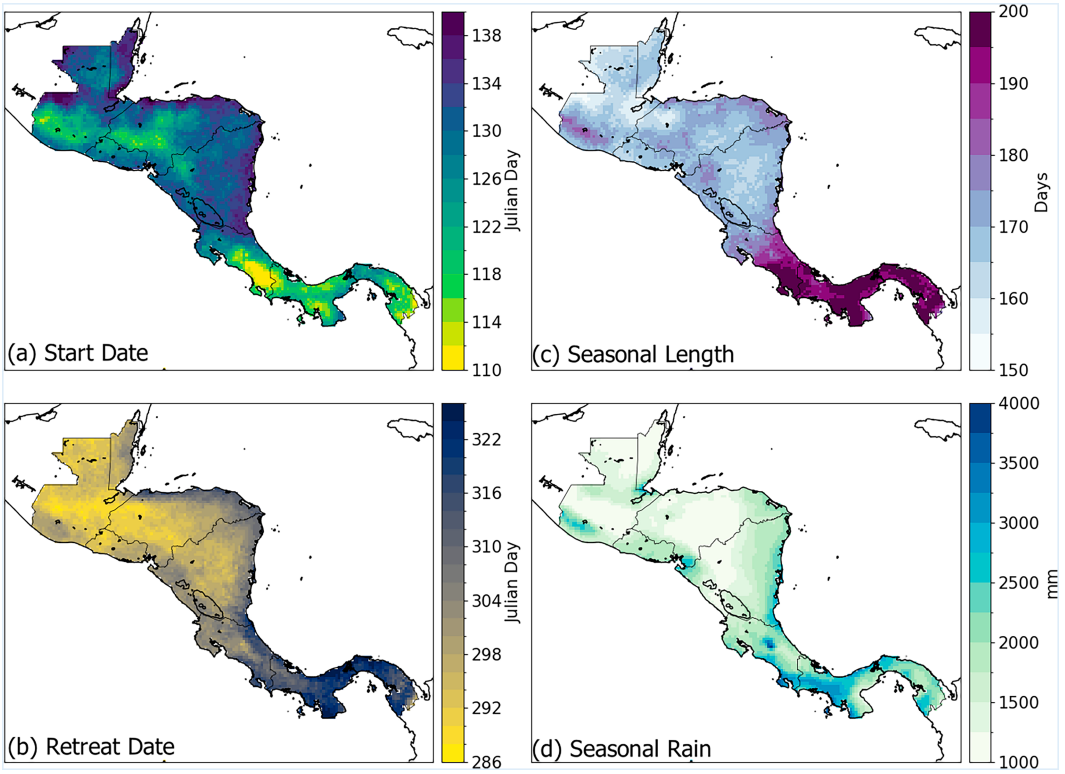

FIG. 2. The 22-yr (2001–22) climatological median of (a) start date (Julian day), (b) retreat date (Julian day), (c) seasonal length (days), and (d) seasonal rain (mm) from 12-h latency IMERG product.

root-mean-square error (RMSE) of the daily climatology of rainfall of IMERG is relatively small (<2 mm day^{-1}) compared to the corresponding climatology in most of the stations. However, comparatively, the wet bias at stations over Honduras (HOM000078708 and HO000078711) and dry bias over El Salvador (MXN000007172) with RMSE of the seasonal cycle at 1.81, 1.76, and 2.19 mm day^{-1}, respectively, are greater than other stations. In terms of variability, the high-amplitude peaks of the daily climatological rainfall in all eight stations are generally underestimated by IMERG (Figs. 1a–f). Biswas and Chandrasekar (2018) indicate that the dual-frequency precipitation radar of the GPM underestimates high rain rates in convective cases. In summary, Fig. 1 suggests that the IMERG product with 12-h latency is a viable product for conducting the proposed analysis for the region that has real-time applications.

b. *Climatology*

Figures 2a–d show the climatological median from 2001 to 2022 of the start and retreat dates, length, and seasonal rainfall of the rainy season. Since an ensemble of 1001 members is generated from the methodology, we have used the median value of the diagnosed start, retreat, length, and seasonal rain for each rainy season to compute this climatology to avoid the influence of outliers. In Fig. 2a, we observe that the start date is generally earlier on the Pacific coast than on the Atlantic coast. Furthermore, the earliest start dates appear in Panama, and start dates gradually occur later in the year as we proceed further north. However, this progression is not uniform with parts of the Pacific coast of Costa Rica, Nicaragua, and El Salvador displaying later start dates compared to parts of Honduras and Guatemala. In fact, the earliest start dates in Fig. 2a appear to be concentrated over the Central American Dry Corridor (CADC) region (Gotlieb et al. 2019). The CADC region is identified along the Pacific littoral from Western Guatemala through northern Costa Rica that has long dry seasons in boreal winter (at least 4 months in duration), is prone to drought, and has a marked MSD (Gotlieb et al. 2019). The west-to-east progression of the start date of the rainy season is, however, more uniform across Central America (Fig. 2a). These patterns of the start date in Fig. 2a match reasonably well with the mean start dates diagnosed from rainfall pentads in Gramzow and Henry (1972). For example, Gramzow and Henry (1972) find the earliest start dates occur near the southern Pacific coast of Costa Rica, as shown in Fig. 2a. Similarly, the coast of Panama along the Gulf of Parita has the latest start date than the rest of Panama (Fig. 2a) as in Nakaegawa et al. (2015). Alfaro (2000) also showed that earlier start dates appear in the south and later start dates in the north.

Similarly, the retreat date shows a meridional and a zonal gradient in Fig. 2b. For example, the later retreat dates in Panama and Costa Rica compared to the rest of Central America are apparent. Furthermore, the Caribbean coast of Central America displays a later retreat date than the Pacific

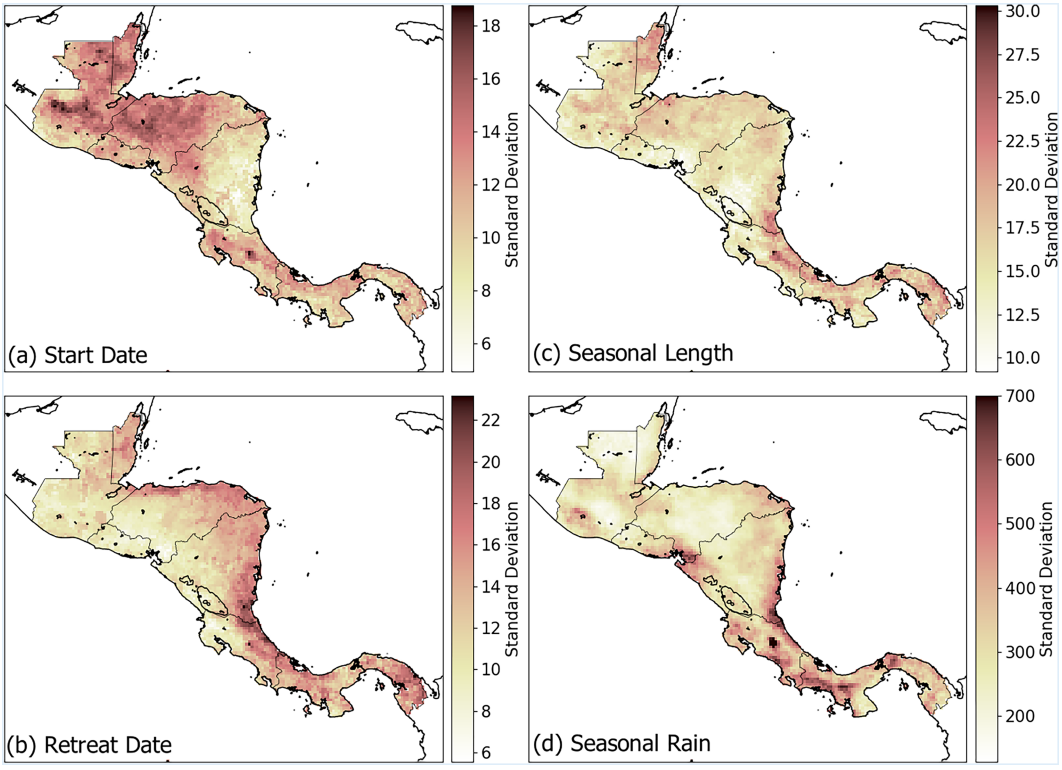

FIG. 3. The standard deviation of (a) start date (days), (b) retreat date (days), (c) seasonal length (days), and (d) seasonal rain (mm) of the wet season.

coast, with interior areas in Nicaragua, Honduras, and Guatemala showing some of the earliest retreat dates of the rainy season (Fig. 2b). Again, the retreat dates in Fig. 2b are consistent with those shown in Gramzow and Henry (1972). For example, Gramzow and Henry (1972) show that the earliest retreat dates occur over the mountains of Guatemala and Honduras as shown in Fig. 2b.

Consequently, the length of the rainy season is the longest in Panama and parts of Costa Rica from a relatively earlier start and a later retreat date of the rainy season (Fig. 2c). Climatologically, some of the shortest rainy seasons are in Belize and in the interiors of Guatemala, Honduras, and Nicaragua (Fig. 2c). Interestingly, the shortest rainy season in Fig. 2c is not aligned with the CADC boundary. In fact, many locations in the CADC region display a similar seasonal length as those along the Caribbean coast at the same latitudes (Fig. 2c). It is this spatial variation of the length of the season that is often missed when rainy seasons are fixed to calendar months across Central America.

The corresponding climatological seasonal mean rainfall, accumulated from the start to the retreat day of the rainy season is shown in Fig. 2d. Generally, longer seasons correspond to higher seasonal rain in Panama and Costa Rica. However, the correspondence between the length of the season (Fig. 2c) and the seasonal rain (Fig. 2d) is not so obvious with parts of Panama and Costa Rica displaying far less seasonal rain and is comparable to other northern parts of Central America despite its comparatively longer length of the rainy season. This implies that the daily rain rates in the rainy season are relatively weaker in some of these regions in Panama and Costa Rica. We also observe that the interiors of Nicaragua, Honduras, and Guatemala besides Belize receive some of the lowest seasonal rain in the rainy season compared to other parts of Central America. Many of these regions coincide with CADC region, which has a distinct MSD that tend to reduce the seasonal total rainfall (Peralta Rodríguez et al. 2012; Gotlieb et al. 2019).

c. *Interannual variability*

The four variables shown in Fig. 2 display considerable variability as noted by their standard deviation (Fig. 3). Furthermore, the standard deviation exhibits strong spatial gradients in the variations of the start date, retreat date, length, and seasonal rain of the rainy season (Fig. 3). It is interesting to note that regions of small and large interannual variations of the start date (Fig. 3a), retreat date (Fig. 3b), length of the season (Fig. 3c), and season rain (Fig. 3d) are generally coincident with the earliest and latest climatological start (Fig. 2a) and retreat (Fig. 2b) dates, shortest and longest seasonal length (Fig. 2c), and driest and wettest seasonal rainfall (Fig. 2d), respectively. Therefore, accounting for the variations in the length of the season and their impact on the seasonal rain of the rainy season at local or small spatial scales is important. In Fig. 4a, we show the correlations of the median start date (diagnosed from the 1001 ensemble members) with the corresponding median seasonal length of the rainy season. The

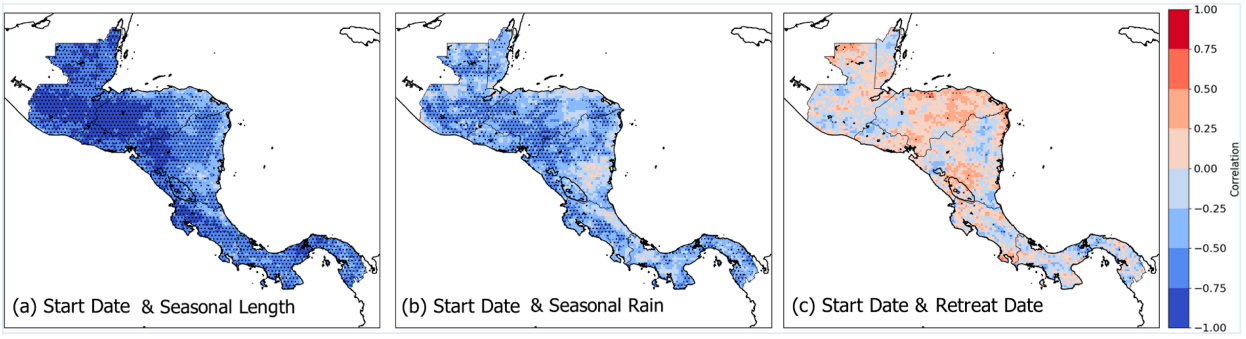

FIG. 4. The correlations of the anomalies of the median start date with anomalies of the median of (a) seasonal length, (b) seasonal rain, and (c) seasonal retreat date. The statistically significant values at a 5% significance level according to the *t* test are stippled.

correlations are significantly large and negative except near the Caribbean coast of Nicaragua and Honduras (Fig. 4a). The negative correlations in Fig. 4a suggest that a longer or shorter rainy season is associated with an early or later start date of the rainy season, respectively. Furthermore, in Fig. 4b, we show the correlations of the start date with the corresponding seasonal rainfall anomaly of the rainy season, which yet again highlights the importance of the start date variations. The regions of Central America that exhibit statistically significant correlations in Fig. 4b suggest that a wetter or drier rainy season is associated with an early or a later start of the rainy season, respectively. Some of the highest correlations between the start date and seasonal length (Fig. 4a) and total seasonal rain (Fig. 4b) fall within the CADC region, which is particularly vulnerable to rainfall variability. However, the statistically significant correlations between the start and the retreat dates are isolated and rare (Fig. 4c). This implies that the influence of the start date variations on the length and the seasonal rain of the rainy season is relatively independent of the influence of the retreat date variations. In summary, the relationships in Fig. 4 suggest that monitoring the start date of the rainy season has the benefit of providing an outlook of the forthcoming length and seasonal rainfall anomaly of the rainy season over most of Central America.

Similarly, the correlations of the retreat date variations with the corresponding anomalies of the length of the rainy season are shown in Fig. 5a. On comparing Figs. 4a and 5a, we notice that there is significant overlap in the regions where the retreat and start date variations affect the seasonal length. The fractional number of grid points with significant correlation that overlaps between Figs. 4a and 5a is 86%. However, more subtly, we find that in some of the regions along the Caribbean coasts of Nicaragua and Honduras, the retreat date variations have a significant correlation with the length of the rainy season (Fig. 5a) compared to the insignificant correlations between the start date and length of the rainy season in Fig. 4a. In contrast, over western Honduras, the correlations between the start date and the seasonal length are relatively significant (Fig. 4a) while the correlations between retreat date and length of the season are weak (Fig. 5a). But given that in many of these regions the covariability between the start and retreat dates are weak (Fig. 4c), their corresponding influence on the seasonal length and seasonal rain are independent of each other. The statistically significant positive correlations in Fig. 5a suggest that early or later retreat of the rainy season is associated with shorter or longer length of the rainy season, respectively.

Likewise, the positive correlations of retreat date with seasonal rain over Panama, Costa Rica, parts of the Caribbean coast of Nicaragua and Honduras, and Belize suggest that early or later retreat is associated with drier or wetter rainy seasons, respectively (Fig. 5b). It is apparent from comparing

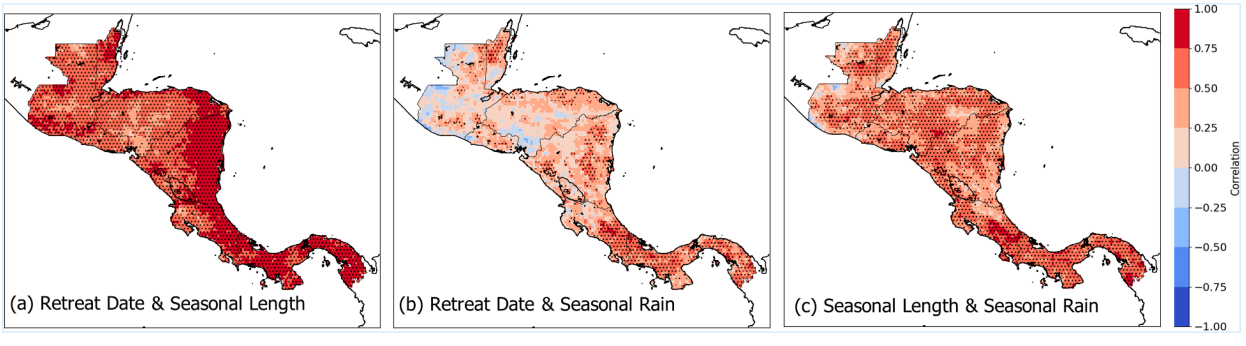

FIG. 5. The correlations of the anomalies of the median retreat date with anomalies of the median of (a) seasonal length and (b) seasonal rain of the rainy season. (c) The correlations of the seasonal length with corresponding seasonal rainfall anomalies of the rainy season. The statistically significant values at a 5% significance level according to the *t* test are stippled.

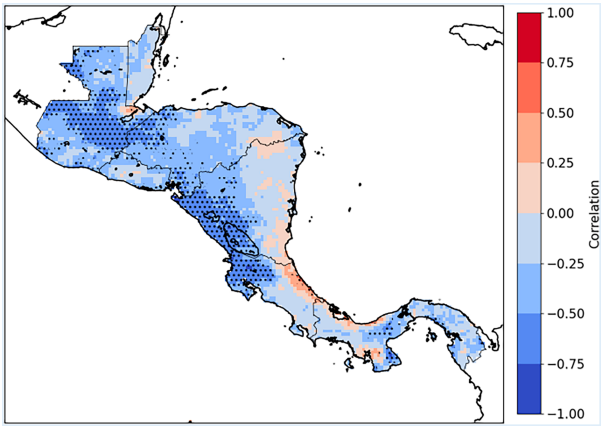

FIG. 6. The correlation of JJA Niño3.4 SST index (OISSTv2; Reynolds et al. 2002) with anomalies of seasonal rain of the rainy season. The statistically significant values at a 5% significance level according to the *t* test are stippled. Field significance at the 95% confidence level following Livezey and Chen (1983) is verified.

Figs. 4b and 5b that the regions of overlap with significant correlations are relatively small. In fact, the fractional number of grid points with significant correlation that overlaps between Figs. 4b and 5b is 10%. For example, the correlations in Fig. 4b over interior Honduras, Guatemala, and the west coast of Nicaragua are strong, while it is weak in Fig. 5b, suggesting that variations in start and retreat dates complement each other in associating with the corresponding changes in the seasonal rainfall. However, from the diagnosed relationships in Figs. 4 and 5, it is apparent that unlike start date variations which can potentially indicate the length and seasonal anomaly of the upcoming rainy season, the retreat date variations can only posteriorly explain the seasonal rainfall anomalies of the wet season. Nonetheless, the seasonal length anomalies have a widespread and significant relationship with seasonal rain of the rainy season across Central America (Fig. 5c). There are some exceptions, however, where the length of the season variation does not covary significantly with seasonal rain (Fig. 5c). For example, in the region bordering between Costa Rica and Nicaragua, parts of Caribbean coasts of Nicaragua and Honduras, and some parts of Guatemala, neither the start date (Figs. 4b and 5c) nor the retreat date (Figs. 5b,c) variations have a significant influence on the seasonal rain.

The correlations in Figs. 4a and 4b and in Figs. 5a and 5b assume significance in the fact that other potential remote forcings like the ENSO variability (Fig. 6), the tropical Atlantic warm pool (Fig. S4a), the tropical North Atlantic index (Figs. S4a,b), interbasin tropical Atlantic–Pacific SST gradient (Fig. 7), and the tropical northeast Pacific warm pool (not shown) have comparatively weaker and spatially less extensive correlations with the seasonal variations of the rainy season of Central America. In fact, the correlations of the mean MAM ENSO index with seasonal rain and mean JJA ENSO index with retreat date and seasonal length fail the field significance test (not shown). However, like the earlier studies (e.g., Enfield and Alfaro 1999), we find that parts of the Pacific slope of Central America display a negative correlation between the seasonal rainfall and the preceding seasonal mean JJA ENSO index (Fig. 6). Earlier studies indicate that ENSO tends to have a high correlation with rainfall on the Pacific coast in the late rainy season while the tropical North Atlantic Ocean has a stronger influence in the early part of the rainy season (Enfield and Alfaro 1999; Giannini et al. 2000; Amador et al. 2016a). These signals, however, tend to get obfuscated for total seasonal anomalies of rainfall spanning the rainy season, thereby limiting the seasonal predictability of the wet season hydroclimate in the region. This could also be a potential reason for the insignificant relationship between the start and retreat date variations, reflecting the evolution of the large-scale teleconnections with the early and later parts of the rainy season of Central America (Wang 2007; Amador 2008; Durán-Quesada et al. 2017). We see that correlations between the seasonal rain and ENSO index strengthen as we use the JJA season for the latter instead of the MAM season (not shown but fails the field significance test). This is because the correlations

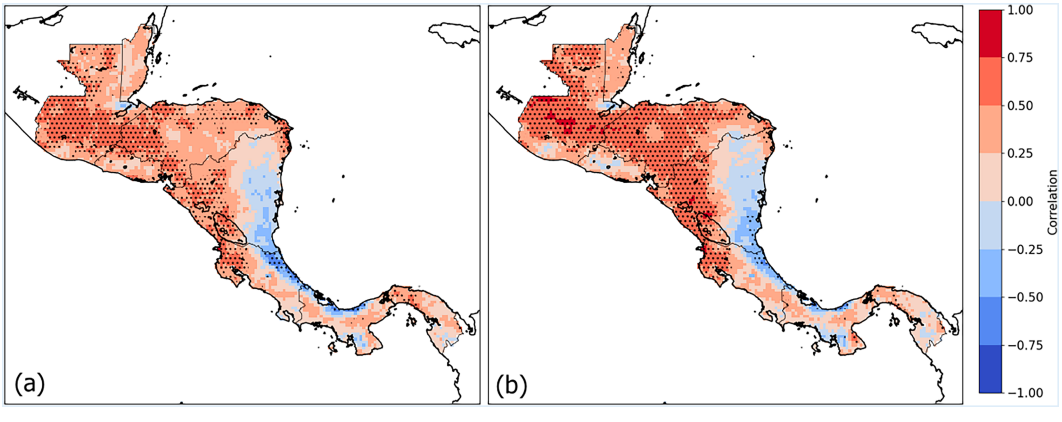

FIG. 7. The correlation of the seasonal rain of the rainy season with (a) MAM and (b) JJA interbasin tropical Atlantic–Pacific SST index following Kim et al. (2020) using OISSTv2 (Reynolds et al. 2002) The statistically significant values at a 5% significance level according to the *t* test are stippled. Field significance at the 95% confidence level following Livezey and Chen (1983) is verified.

are nearly contemporaneous and many studies suggest a strong modulation of the Caribbean low-level jet by ENSO in JJA, which is one of the main sources of moisture supply to the Central American monsoon. It should be noted that the preceding DJF ENSO index anomalies also have an insignificant relationship to wet season variations of Central America (not shown).

We also examined the teleconnections of the Central American rainy season variability with the interbasin gradient of SST between the tropical Atlantic and Pacific Oceans (Fig. 7; Alfaro et al. 1998; Enfield and Alfaro 1999; Alfaro and Cid 1999a,b; Kim et al. 2020). The theory for this observed teleconnection (Fig. 7) is the modulation of the Walker circulation, which results in a wetter or a drier rainy season when the northern tropical Atlantic is warmer or colder than tropical Pacific Ocean (Enfield and Alfaro 1999; Misra et al. 2014), respectively. We similarly observe positive correlations in Figs. 7a and 7b between the seasonal rainfall anomalies and the interbasin SST gradient for MAM and JJA, which develop more strongly from boreal spring to summer season, respectively. However, the correlations of the interbasin SST gradient with the start date, retreat date, and seasonal length fail the field significance test (not shown). Furthermore, the correlations of the near-contemporaneous JJA interbasin index (Fig. 7b) are far stronger than with the MAM interbasin index (Fig. 7a). The correlations of the seasonal rain with the MAM and JJA tropical North Atlantic SST in Figs. S4b and S4c also show similar correlations as Figs. 7a and 7b, respectively, suggesting its dominating influence. A few studies have shown that as the north tropical Atlantic warms anomalously in boreal spring and summer seasons, the Caribbean low-level jet weakens and increases the moisture flux convergence over Central America, thereby making the Central American monsoon anomalously wetter (Wang et al. 2008; Misra et al. 2014; Hidalgo et al. 2017). Similarly, as the anomalous SST gradient between the tropical Atlantic and eastern Pacific develops, the low-level easterlies also get modulated, thereby affecting the moisture flux convergence in the isthmus. However, the relationships of the tropical North Atlantic index with the onset/retreat dates and length of the season are insignificant (not shown). The correlations of the seasonal rain with the Atlantic warm pool index are limited to Costa Rica and Panama (Fig. S4a), while the correlations with the tropical northeast Pacific warm pool index are insignificant (not shown). Therefore, the local correlations in Figs. 4 and 5 in comparison to Figs. 6 and 7, and Fig. S4 capture the variations that dictate the seasonal evolution of the rainy season over Central America far more extensively and robustly. As Figs. 6 and 7 and Fig. S4 suggest, many large-scale climate drivers affect regional rainfall over Central America, often with complex interactions, making it difficult to predict the seasonal anomalies of the length or seasonal rainfall using these teleconnections alone. However, once an onset date of the rainy season is established, then this metric alone can be more indicative of both the length and total seasonal rainfall anomaly than predicting how the climate drivers will interact to affect the quantity and duration of upcoming seasonal rainfall over Central America.

d. Real-time monitoring

In Central America, the Regional Climate Outlook Forum (RCOF; set up by the WMO in the late 1990s to produce consensus-based regional climate outlooks based on climate predictions from all regional participants; Daly and Dessai 2018) typically uses statistical models using tropical SST as predictors for seasonal prediction (e.g., Alfaro 2007; Fallas López and Alfaro 2012a,b) or uses MOS, where statistical corrections are applied to dynamical model output (e.g., Recalde-Coronel et al. 2014; Alfaro et al. 2018). Kowal et al. (2023) suggest that dynamical climate models also offer reasonable seasonal prediction skills in the region that complement the statistical models. However, RCOF in Central America focuses its effort on the May–June–July, August–September–October, and December–January–February–March seasons associated with the first planting (or Primera) season (García-Solera and Ramírez 2012), annual maximum rainfall period, and winter seasons, respectively. In this study, we are targeting the entire rainy season rainfall anomalies that overlap with the Primera and the annual maximum rainfall periods. One of the objectives of this paper is to leverage the local relationships displayed in Fig. 4 to provide a seasonal outlook on seasonal precipitation anomalies and seasonal length of the rainy season by monitoring the start date variations of the rainy season. In Fig. 8, we show the AROC for the outlook of the seasonal length and seasonal rainfall anomalies based on anomalous early and late-start seasons. The anomalous start dates, length of the season, and seasonal rain are considered when they are not in the middle but extreme terciles. In Fig. 8a, we find that the outlook of a long rainy season from an early start has a very high AROC, well over 0.5 across Central America, with rare exceptions in pockets over Costa Rica and along the Caribbean coasts of Nicaragua and Honduras. Similarly, the outlook of the wetter season in early start seasons also shows AROC $\geq$ 0.5, widespread across Central America (Fig. 8b). However, the AROC scores in Fig. 8b are weaker and slightly less widespread than in Fig. 8a suggesting that the prognostic skill of early start seasons in dictating longer length of the season is stronger than the seasonal rainfall anomaly.

Similarly, the outlook of the short rainy season from the late start is also promising (Fig. 8c). In comparison to Fig. 8a, however, Fig. 8c has much higher AROC scores over Guatemala, El Salvador, and Belize suggesting higher probabilistic skills in anticipating shorter rainy season from late-start seasons. Likewise, the outlook of drier rainy seasons during late-start years has higher AROC and is slightly more widespread across Central America (Fig. 8d) compared to wetter seasons in early start years (Fig. 8b). The late-start date seems to be an especially good warning for a shorter (Fig. 8d) and drier (Fig. 8e) season in the CADC region, which is especially vulnerable to drought and water insecurity (Gotlieb et al. 2019).

The outlook for normal (middle tercile) seasonal length and seasonal rain has the weakest skill compared to anomalous years (Figs. 8e,f). The AROC scores for the outlook of a normal length of the season (in the middle tercile) during a normal-start (middle tercile) season is the weakest (Fig. 8e)

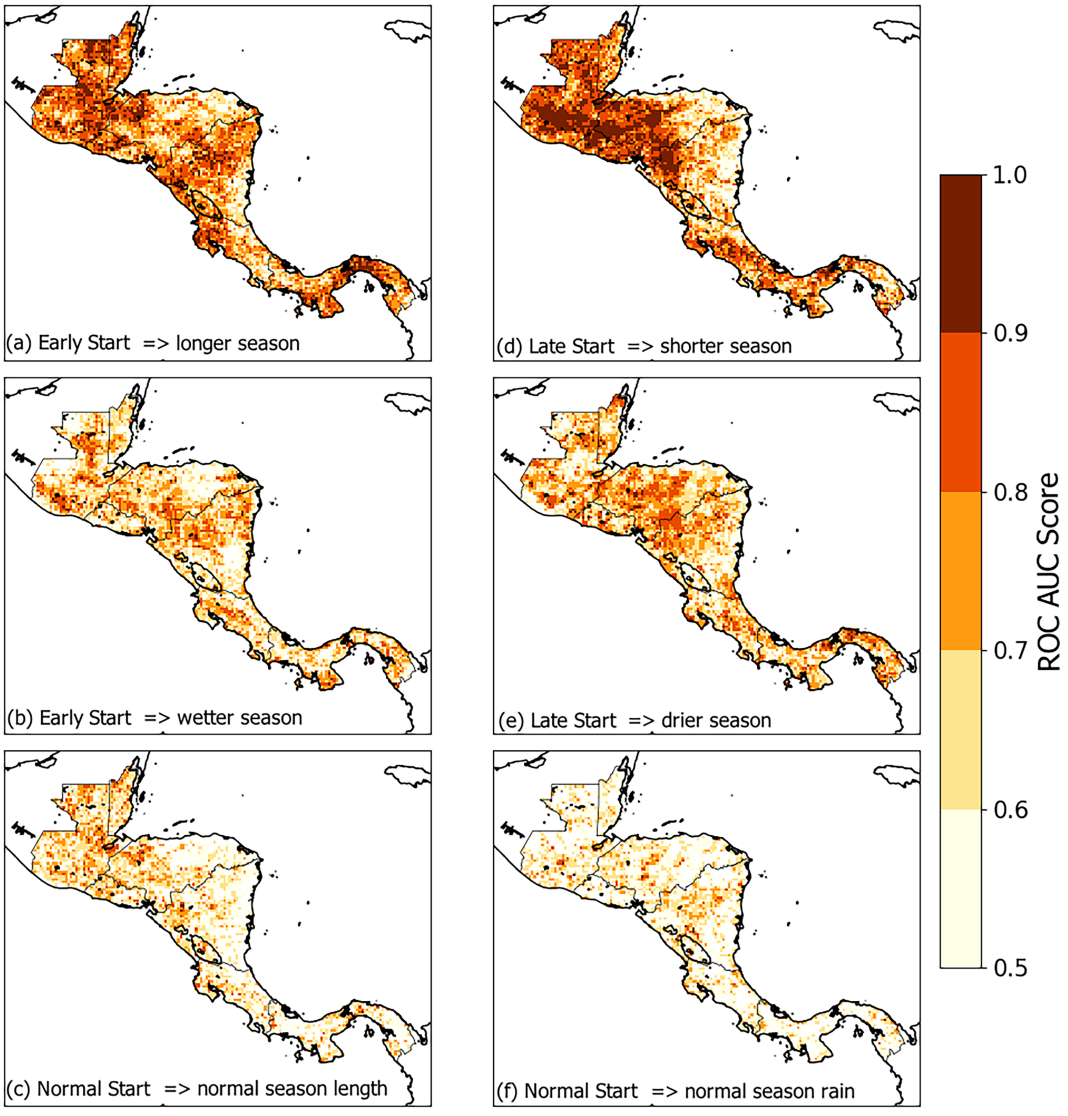

FIG. 8. AROC curve for the outlook of (a) a longer rainy season and (b) a wetter rainy season based on an early start, (d) a shorter wet season and (e) a drier rainy season based on the late start of the rainy season, and (c) a normal rainy season length and (f) a normal rainy season rainfall based on normal start of the rainy season. Only regions with an AROC curve ≥ 0.5, which signifies probabilistic skill that is better than random forecast, are shaded.

compared to anomalous start seasons (Figs. 8a,c). Similarly, the AROC scores for the outlook of normal seasonal rain during a normal-start season are weak (Fig. 8f) compared to anomalous seasons (Figs. 8b,d). Nonetheless, normal-start seasons do display some useful skill that is widespread across Central America.

4. Conclusions

Central America with its complex geography of an isthmus, steep orography, and diverse vegetation features offers a stiff challenge to predict its hydroclimate at all spatial and temporal scales. While many climate mechanisms are significant drivers of rainfall over the region, their complex interactions with each other and the diverse topography can make it difficult to pinpoint exactly how rainfall will evolve for a given location. We show how using a simple but robust estimate of the start date of the rainy season can provide a useful indicator of the length and seasonal rainfall of the rainy season. This method is especially useful for regions like the CADC region, as a delayed start can serve as a reliable warning for a shorter and drier rainy season for this drought-prone subregion of the isthmus.

Our study, unlike most other previous studies, spans the entire rainy season across the MSD periods. Many of the earlier studies target the early and late rain periods of the rainy season separately with the large-scale climate drivers like tropical North Atlantic SST, ENSO, and interocean basin index being strongly leveraged for their predictability. Our study nicely

complements these earlier efforts as predicting the entire rainy season is also useful in providing more lead time for planning for an anomalous season. The proposed methodology includes the variations in the length of the season in accounting for the variability of the rainy season that is otherwise ignored in the fixed calendar month definitions of the season. We show that the variations in the start and retreat dates of the rainy season over Central America influence the length and the seasonal rainfall variations of the rainy season significantly. Furthermore, the impact of start and retreat date variations on the corresponding seasonal length and seasonal rainfall is found to be relatively independent of each other. With the availability of high-resolution rainfall data like IMERG, the proposed methodology can easily and effectively be adapted for real-time monitoring of the evolution of the rainy season over this region.

In this study, we also verify the seasonal cycle of the IMERG rainfall analysis in the region with available in situ data. The IMERG rainfall analysis used in the study shows reasonable fidelity for its application in monitoring the seasonal evolution of the precipitation over Central America.

This study offers a very simple but effective tool to provide a probabilistic outlook of the forthcoming rainy season by simply monitoring the realization of the start date of the rainy season. The methodology, by way of generating an ensemble of time series of daily rainfall from perturbing the original time series of daily rainfall at each grid point separately, provides a corresponding ensemble of start and retreat dates, seasonal length, and seasonal rain of the rainy season. We show that across most of the region in Central America, an early or later start date of the rainy season is closely associated with a longer and wetter or a shorter and drier seasonal length and rainfall anomaly of the rainy season, respectively. The probabilistic skill scores of such an outlook presented in this study also support the effectiveness of this local teleconnection. Therefore, the proposed monitoring of the local start of the rainy season would be beneficial and complimentary to existing efforts, especially in the presence of stiff challenges to seasonal prediction for the region.

Acknowledgments. We thank the three anonymous reviewers for their very useful comments and suggestions on an earlier version of the manuscript. We acknowledge the support from NASA Grant 80NSSC22K0595. The IMERG dataset was provided by the NASA/Goddard Space Flight Center and PPS which developed and computed the IMERG as a contribution to GPM and archived at the NASA GES DISC.

Data availability statement. The IMERG rainfall from NASA was obtained from https://gpm1.gesdisc.eosdis.nasa.gov/data/GPM_L3/GPM_3IMERGDL.06/. The NOAA's Global Historical Climatology Network (GHCN) data were obtained from https://www.ncei.noaa.gov/products/land-based-station/global-historical-climatology-network-daily. The OISST version 2 data used for the analysis in this study are available at https://psl.noaa.gov/data/gridded/data.noaa.oisst.v2.highres.html. The python code to compute the onset/demise dates in the paper is available at https://osf.io/bmgyj/. All the figures were generated by using Python (Van Rossum and Drake 2009).

REFERENCES

Alfaro, E. J., 2000: Eventos cálidos y fríos en el Atlántico tropical norte. *Atmósfera*, **13**, 109–119.

——, 2002: Some characteristics of the annual precipitation cycle in Central America and their relationship with its surrounding tropical oceans (in Spanish). *Top. Meteor. Oceanogr.*, **9**, 88–103.

——, 2007: Uso del análisis de correlación canónica para la predicción de la precipitación pluvial en Centroamérica. *Rev. Ing. Compet.*, **9**, 33–48.

——, 2014: Caracterizacion del "veranillo" en dos cuencas de la vertiente del Pacifico de Costa Rica, America Central. *Rev. Biol. Trop.*, **62** (Suppl. 4), 1–15, https://doi.org/10.15517/rbt.v62i4.20010.

——, and L. Cid, 1999a: Ajuste de un modelo VARMA para los campos de anomalías de precipitación en Centroamérica y los índices de los océanos Pacífico y Atlántico tropical. *Atmósfera*, **13**, 205–222.

——, and ——, 1999b: Análisis de las Anomalías en el inicio y el término de la estación lluviosa en Centroamérica y su relación con los océanos Pacífico y Atlántico tropical. *Tóp. Meteor. Oceanogr.*, **6**, 1–13.

——, ——, and D. B. Enfield, 1998: Relaciones entre el inicio y el término de la estación lluviosa en Centroamérica y los Océanos Pacífico y Atlántico tropical. *Investig. Mar.*, **26**, 59–69, https://doi.org/10.4067/S0717-71781998002600006.

——, X. Chourio, Á. G. Muñoz, and S. J. Mason, 2018: Improved seasonal prediction skill of rainfall for the Primera season in Central America. *Int. J. Climatol.*, **38**, e255–e268, https://doi.org/10.1002/joc.5366.

Amador, J. A., 2008: The intra-Americas sea low-level jet: Overview and future research. *Ann. N. Y. Acad. Sci.*, **1146**, 153–188, https://doi.org/10.1196/annals.1446.012.

——, E. J. Alfaro, O. G. Lizano, and V. O. Magaña, 2006: Atmospheric forcing of the eastern tropical Pacific: A review. *Prog. Oceanogr.*, **69**, 101–142, https://doi.org/10.1016/j.pocean.2006.03.007.

——, E. R. Rivera, A. M. Durán-Quesada, G. Mora, F. Sáenz, B. Calderón, and N. Mora, 2016a: The easternmost tropical Pacific. Part I: A climate review. *Rev. Biol. Trop.*, **64** (S1), 1–22, https://doi.org/10.15517/rbt.v64i1.23407.

——, A. M. Durán-Quesada, E. R. Rivera, G. Mora, F. Sáenz, B. Calderón, and N. Mora, 2016b: The easternmost tropical Pacific. Part II: Seasonal and intraseasonal modes of atmospheric variability. *Rev. Biol. Trop.*, **64**, 23–57, https://doi.org/10.15517/rbt.v64i1.23409.

Bhardwaj, A., and V. Misra, 2019: Monitoring the Indian summer monsoon evolution at the granularity of the Indian meteorological sub-divisions using remotely sensed rainfall products. *Remote Sens.*, **11**, 1080, https://doi.org/10.3390/rs11091080.

Biswas, S. K., and V. Chandrasekar, 2018: Cross-validation of observations between the GPM dual-frequency precipitation radar and ground based dual-polarization radars. *Remote Sens.*, **10**, 1773, https://doi.org/10.3390/rs10111773.

Bombardi, R. J., J. L. Kinter III, and O. W. Frauenfeld, 2019: A global gridded dataset of the characteristics of the rainy and dry seasons. *Bull. Amer. Meteor. Soc.*, **100**, 1315–1328, https://doi.org/10.1175/BAMS-D-18-0177.1.

Cid-Serrano, L., S. M. Ramirez, E. J. Alfaro, and D. B. Enfield, 2015: Analysis of the Latin American west coast rainfall predictability using an ENSO index. *Atmósfera*, **28**, 191–203, https://doi.org/10.20937/ATM.2015.28.03.04.

Dai, A., and T. M. L. Wigley, 2000: Global patterns of ENSO induced precipitation. *Geophys. Res. Lett.*, **27**, 1283–1286, https://doi.org/10.1029/1999GL011140.

Daly, M., and S. Dessai, 2018: Examining the goals of the regional climate outlook forums: What role for user engagement? *Wea. Climate Soc.*, **10**, 693–708, https://doi.org/10.1175/WCAS-D-18-0015.1.

Dunning, C. M., E. C. L. Black, and R. P. Allan, 2016: The onset and cessation of seasonal rainfall over Africa. *J. Geophys. Res. Atmos.*, **121**, 11 405–11 424, https://doi.org/10.1002/2016JD025428.

Durán-Quesada, A. M., L. Gimeno, and J. Amador, 2017: Role of moisture transport for Central American precipitation. *Earth Syst. Dyn.*, **8**, 147–161, https://doi.org/10.5194/esd-8-147-2017.

——, R. Sori, P. Ordoñez, and L. Gimeno, 2020: Climate perspectives in the intra–Americas seas. *Atmosphere*, **11**, 959, https://doi.org/10.3390/atmos11090959.

Enfield, D. B., and E. J. Alfaro, 1999: The dependence of Caribbean rainfall on the interaction of the tropical Atlantic and Pacific Oceans. *J. Climate*, **12**, 2093–2103, https://doi.org/10.1175/1520-0442(1999)012<2093:TDOCRO>2.0.CO;2.

Fallas López, B., and E. J. Alfaro, 2012a: Uso de herramientas estadísticas para la predicción estacional del campo de precipitación en América Central como apoyo a los Foros Climáticos Regionales. 1: Análisis de tablas de contingencia. *Rev. Climatol.*, **12**, 61–79.

——, and ——, 2012b: Uso de herramientas estadísticas para la predicción estacional del campo de precipitación en América Central como apoyo a los Foros Climáticos Regionales. 2: Análisis de correlación canónica. *Rev. Climatol.*, **12**, 93–105.

Flatau, M. K., P. J. Flatau, J. Schmidt, and G. N. Kiladis, 2003: Delayed onset of the 2002 Indian monsoon. *Geophys. Res. Lett.*, **30**, 1768, https://doi.org/10.1029/2003GL017434.

García-Solera, I., and P. Ramírez, 2012: Central America's seasonal outlook forum. The Climate Services Partnership, 8 pp.

Giannini, A., Y. Kushnir, and M. A. Cane, 2000: Interannual variability of Caribbean rainfall, ENSO, and the Atlantic Ocean. *J. Climate*, **13**, 297–311, https://doi.org/10.1175/1520-0442(2000)013<0297:IVOCRE>2.0.CO;2.

Giraldo-Mendez, D., D. Martínez-Baron, A. M. Loboguerrero, T. Gumucio, J. D. Martínez, and J. Ramírez-Villegas, 2019: Technical agroclimatic committees (MTA): A detailed guide for implementing, step-by-step. CGIAR Research Program on Climate Change, Agriculture and Food Security (CCAFS), 53 pp., https://hdl.handle.net/10568/105442.

Gotlieb, Y., P. Pérez-Briceño, H. Hidalgo, and E. Alfaro, 2019: The Central American dry corridor: A consensus statement and its background. *Rev. Yu'am*, **3**, 42–51.

Gramzow, R. H., and W. K. Henry, 1972: The rainy pentads of Central America. *J. Appl. Meteor.*, **11**, 637–642, https://doi.org/10.1175/1520-0450(1972)011<0637:TRPOCA>2.0.CO;2.

Hidalgo, H. G., J. A. Amador, E. J. Alfaro, and B. Quesada, 2013: Hydrological climate change projections for Central America. *J. Hydrol.*, **495**, 94–112, https://doi.org/10.1016/j.jhydrol.2013.05.004.

——, A. M. Durán-Quesada, J. A. Amador, and E. J. Alfaro, 2015: The Caribbean low-level jet, the inter-tropical convergence zone and precipitation patterns in the intra-Americas sea: A proposed dynamical mechanism. *Geogr. Ann.*, **97A**, 41–59, https://doi.org/10.1111/geoa.12085.

——, E. J. Alfaro, and B. Quesada-Montano, 2017: Observed (1970–1999) climate variability in Central America using a high-resolution meteorological dataset with implication to climate change studies. *Climatic Change*, **141**, 13–28, https://doi.org/10.1007/s10584-016-1786-y.

Huffman, G. J., E. F. Stocker, D. T. Bolvin, E. J. Nelkin, and J. Tan, 2019: GPM IMERG final precipitation L3 half hourly 0.1 degree × 0.1 degree V06 at GES DISC. Goddard Earth Sciences Data and Information Services Center (GES DISC), accessed 7 July 2021, https://doi.org/10.5067/GPM/IMERG/3B-HH/06.

Jayasankar, C. B., S. Surendran, and K. Rajendran, 2015: Robust signals of future projections of Indian summer monsoon rainfall by IPCC AR5 climate models: Role of seasonal cycle and interannual variability. *Geophys. Res. Lett.*, **42**, 3513–3520, https://doi.org/10.1002/2015GL063659.

Kim, D., S.-K. Lee, H. Lopez, G. R. Foltz, V. Misra, and A. Kumar, 2020: On the role of Pacific-Atlantic SST contrast and associated Caribbean Sea convection in August–October U.S. regional rainfall variability. *Geophys. Res. Lett.*, **47**, e2020GL087736, https://doi.org/10.1029/2020GL087736.

Kowal, K. M., L. J. Slater, A. G. López, and A. F. Van Loon, 2023: A comparison of seasonal rainfall forecasts over Central America using dynamic and hybrid approaches from Copernicus Climate Change Service seasonal forecasting system and the North American Multimodel Ensemble. *Int. J. Climatol.*, **43**, 2175–2199, https://doi.org/10.1002/joc.7969.

Liebmann, B., and J. Marengo, 2001: Interannual variability of the rainy season and rainfall in the Brazilian Amazon basin. *J. Climate*, **14**, 4308–4318, https://doi.org/10.1175/1520-0442(2001)014%3C4308:IVOTRS%3E2.0.CO;2.

Liu, C., and E. Zipser, 2013: Regional variation of morphology of organized convection in the tropics and subtropics. *J. Geophys. Res. Atmos.*, **118**, 453–466, https://doi.org/10.1029/2012JD018409.

——, and ——, 2015: The global distribution of largest, deepest, and most intense precipitation systems. *Geophys. Res. Lett.*, **42**, 3591–3595, https://doi.org/10.1002/2015GL063776.

Livezey, R. E., and W. Y. Chen, 1983: Statistical field significance and its determination by Monte Carlo techniques. *Mon. Wea. Rev.*, **111**, 46–59, https://doi.org/10.1175/1520-0493(1983)111<0046:SFSAID>2.0.CO;2.

Loboguerrero, A. M., F. Boshell, G. León, D. Martinez-Baron, D. Giraldo, L. R. Mejía, E. Díaz, and J. Cock, 2018: Bridging the gap between climate science and farmers in Colombia. *Climate Risk Manage.*, **22**, 67–81, https://doi.org/10.1016/j.crm.2018.08.001.

Magaña, V., J. A. Amador, and S. Medina, 1999: The mid-summer drought over Mexico and Central America. *J. Climate*, **12**, 1577–1588, https://doi.org/10.1175/1520-0442(1999)012<1577:TMDOMA>2.0.CO;2.

Maldonado, T., A. Rutgersson, E. Alfaro, J. Amador, and B. Claremar, 2016: Interannual variability of the midsummer drought in Central America and the connection with sea surface temperatures. *Adv. Geosci.*, **42**, 35–50, https://doi.org/10.5194/adgeo-42-35-2016.

——, E. J. Alfaro, and H. G. Hidalgo, 2018: A review of the main drivers and variability of Central America's climate and seasonal forecast systems. *Rev. Biol. Trop.*, **66** (Suppl. 1), S153–S175.

Martinez, C., L. Goddard, Y. Kushnir, and M. Ting, 2019: Seasonal climatology and dynamical mechanisms of rainfall in

the Caribbean. *Climate Dyn.*, **53**, 825–846, https://doi.org/10.1007/s00382-019-04616-4.

——, Y. Kushnir, L. Goddard, and M. Ting, 2020: Interannual variability of the early and late-rainy seasons in the Caribbean. *Climate Dyn.*, **55**, 1563–1583, https://doi.org/10.1007/s00382-020-05341-z.

Mason, S. J., and N. E. Graham, 1999: Conditional probabilities, relative operating characteristics, and relative operating levels. *J. Climate*, **14**, 713–725, https://doi.org/10.1175/1520-0434(1999)014<0713:CPROCA>2.0.CO;2.

——, and ——, 2002: Areas beneath the relative operating characteristics (ROC) and relative operating levels (ROL) curves: Statistical significance and interpretation. *Quart. J. Roy. Meteor. Soc.*, **128**, 2145–2166, https://doi.org/10.1256/003590002320603584.

Menne, M. J., I. Durre, R. S. Vose, B. E. Gleason, and T. G. Houston, 2012: An overview of the global historical climatology network-daily database. *J. Atmos. Oceanic Technol.*, **29**, 897–910, https://doi.org/10.1175/JTECH-D-11-00103.1.

Misra, V., 2006: Understanding the predictability of seasonal precipitation over Northeast Brazil. *Tellus*, **58A**, 307–319, https://doi.org/10.1111/j.1600-0870.2006.00175.x.

——, and S. DiNapoli, 2014: The variability of the Southeast Asian summer monsoon. *Int. J. Climatol.*, **34**, 893–901, https://doi.org/10.1002/joc.3735.

——, H. Li, and M. Kozar, 2014: The precursors in the Intra-Americas seas to seasonal climate variations over North America. *J. Geophys. Res. Oceans*, **119**, 2938–2948, https://doi.org/10.1002/2014JC009911.

——, D. Groenen, A. Bharadwaj, and A. Mishra, 2016: The warm pool variability of the tropical northeast Pacific. *Int. J. Climatol.*, **36**, 4625–4637, https://doi.org/10.1002/joc.4658.

——, C. B. Jayasankar, P. Beasley, and A. Bhardwaj, 2022: Operational monitoring of the evolution of the rainy season over Florida. *Front. Climate*, **4**, 793959, https://doi.org/10.3389/fclim.2022.793959.

——, S. Dixit, and C. B. Jayasankar, 2023: The regional diagnosis of onset and demise of the rainy season over tropical and subtropical Australia. *Earth Interact.*, **27**, https://doi.org/10.1175/EI-D-22-0026.1.

Murakami, T., L.-X. Chen, A. Xie, and M. L. Shrestha, 1986: Eastward propagation of 30–60 day perturbations as revealed from outgoing longwave radiation data. *J. Atmos. Sci.*, **43**, 961–971, https://doi.org/10.1175/1520-0469(1986)043<0961:EPODPA>2.0.CO;2.

Nakaegawa, T., O. Arakawa, and K. Kamiguchi, 2015: Investigation of climatological onset and withdrawal of the rainy season in Panama based on a daily gridded precipitation dataset with a high horizontal resolution. *J. Climate*, **28**, 2745–2763, https://doi.org/10.1175/JCLI-D-14-00243.1.

Narotsky, C. D., and V. Misra, 2022: The seasonal predictability of the wet season over peninsular Florida. *Int. J. Climatol*, **42**, 3408–3417, https://doi.org/10.1002/joc.7423.

Peralta Rodríguez, O., J. Carrazón Alocén, and C. A. Zelaya Elvir, 2012: *Buenas Prácticas Para la Seguridad Alimentaria y la Gestión De Riesgo*. Organización de las Naciones Unidas para la Alimentación y la Agricultura, 53 pp.

Recalde-Coronel, G. C., A. G. Barnston, and A. G. Muñoz, 2014: Predictability of December–April rainfall in coastal and Andean Ecuador. *J. Appl. Meteor. Climatol.*, **53**, 1471–1493, https://doi.org/10.1175/JAMC-D-13-0133.1.

Reynolds, R. W., N. A. Rayner, T. M. Smith, D. C. Stokes, and W. Wang, 2002: An improved in situ and satellite SST analysis for climate. *J. Climate*, **15**, 1609–1625, https://doi.org/10.1175/1520-0442(2002)015<1609:AIISAS>2.0.CO;2.

Sánchez-Murillo, R., and Coauthors, 2016: Key drivers controlling stable isotope variations in daily precipitation of Costa Rica: Caribbean Sea versus eastern Pacific Ocean moisture sources. *Quat. Sci. Rev.*, **131**, 250–261, https://doi.org/10.1016/j.quascirev.2015.08.028.

Stanski, H. R., L. J. Wilson, and W. R. Burrows, 1989: Survey of common verification methods in meteorology. Research Rep. 89-5, 8 pp., https://www.cawcr.gov.au/projects/verification/Stanski_et_al/VerificationSWBPartI.pdf.

Stewart, I. T., E. P. Maurer, K. Stahl, and K. Joseph, 2022: Recent evidence for warmer and drier growing seasons in climate sensitive regions of Central America from multiple global datasets. *Int. J. Climatol.*, **42**, 1399–1417, https://doi.org/10.1002/joc.7310.

Taylor, M. A., and E. J. Alfaro, 2005: Climate of Central America and the Caribbean. *Encyclopedia of World Climatology*, J. E. Oliver, Eds., Springer, 183–188.

Uehling, J., and V. Misra, 2020: Characterizing the seasonal cycle of the Northern Australian rainy season. *J. Climate*, **33**, 8957–8973, https://doi.org/10.1175/JCLI-D-19-0592.1.

Van Rossum, G., and F. L. Drake, 2009: Python 3 Reference Manual Version 3.12.4. CreateSpace, https://docs.python.org/3/reference/index.html.

Vera, C., and Coauthors, 2006: Toward a unified view of the American monsoon systems. *J. Climate*, **19**, 4977–5000, https://doi.org/10.1175/JCLI3896.1.

Wang, C., 2007: Variability of the Caribbean low-level jet and its relations to climate. *Climate Dyn.*, **29**, 411–422, https://doi.org/10.1007/s00382-007-0243-z.

——, and D. B. Enfield, 2001: The tropical Western Hemisphere warm pool. *Geophys. Res. Lett.*, **28**, 1635–1638, https://doi.org/10.1029/2000GL011763.

——, S.-K. Lee, and D. B. Enfield, 2008: Climate response to anomalously large and small Atlantic warm pools during the summer. *J. Climate*, **21**, 2437–2450, https://doi.org/10.1175/2007JCLI2029.1.

Wani, S. P., T. K. Sreedevi, J. Rockström, and Y. S. Ramakrishna, 2009: Rainfed agriculture-past trends and future prospects. *Rainfed Agriculture: Unlocking the Potential, Comprehensive Assessment of Water Management*, S. P. Wani, J. Rockstrom, and T. Oweis, Eds., Agriculture Series, Vol. 7, CABI, 1–35, https://doi.org/10.1079/9781845933890.0001.

Waylen, P. R., M. E. Quesada, and C. N. Caviedes, 1996: Temporal and spatial variability of annual precipitation in Costa Rica and the Southern Oscillation. *Int. J. Climatol.*, **16**, 173–193, https://doi.org/10.1002/(SICI)1097-0088(199602)16:2%3C173::AID-JOC12%3E3.0.CO;2-R.

WMO, 2000: Standardized Verification System (SVS) for long-range forecasts (LRF). WMO Attachment II.8, 17 pp., https://www.metoffice.gov.uk/binaries/content/assets/metofficegovuk/pdf/research/climate-science/climate-observations-projections-and-impacts/svslrf.pdf.

Zambrano-Bigiarini, M., A. Nauditt, C. Birkel, K. Verbist, and L. Ribbe, 2017: Temporal and spatial evaluation of satellite-based rainfall estimates across the complex topographical and climatic gradients of Chile. *Hydrol. Earth Syst. Sci.*, **21**, 1295–1320, https://doi.org/10.5194/hess-21-1295-2017.

Supplemental Material

Journal of Climate
Using the Observed Variations of the Start Date of the Rainy Season over Central America for Its Reliable Seasonal Outlook
https://doi.org/10.1175/JCLI-D-23-0699.1

Supplementary Material

Using the observed variations of the start date of the rainy season over Central America for its reliable seasonal outlook

Joanna Rodgers[1, 2, 3] Vasubandhu Misra[1, 2, 3, #] and C. B. Jayasankar[2, 3]

[1]Department of Earth, Ocean and Atmospheric Science, Florida State University, Tallahassee, Florida, U. S. A.

[2]Center for Ocean-Atmospheric Prediction Studies, Florida State University, Tallahassee, Florida, U. S. A.

[3]Florida Climate Institute, Florida State University, Tallahassee, Florida, U. S. A.

#Corresponding Author: vmisra@fsu.edu

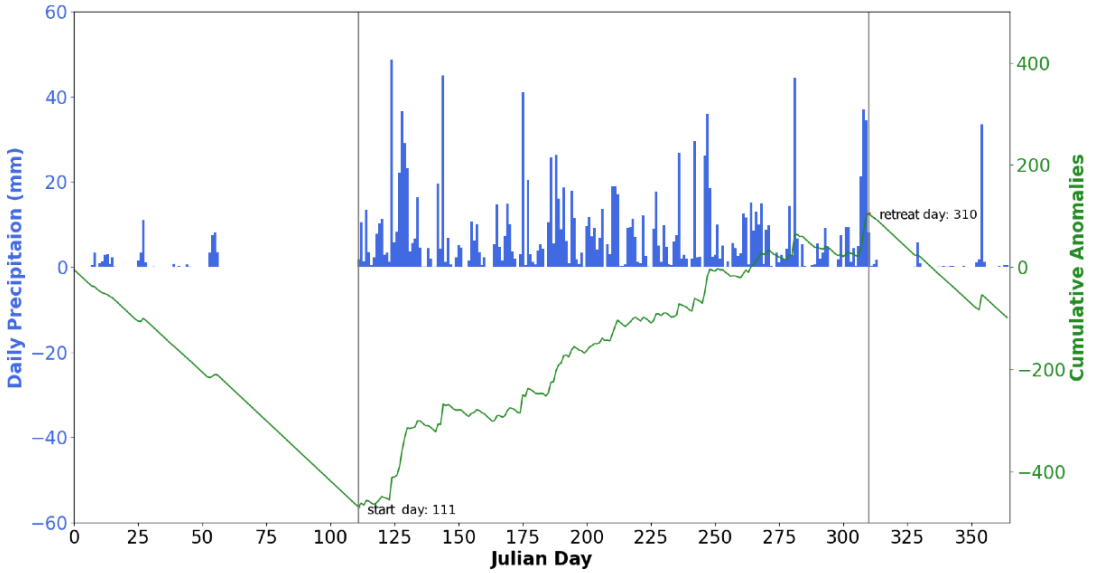

Figure S1: A schematic illustration of the time series of daily rainfall (blue bars; mm day^{-1}) and its corresponding cumulative daily anomaly curve (see Equation 1 in main text; green line; mm) over a specific grid point over Nicaragua for the year 2009. The start (Julian Day 111 or April 21) and retreat (Julian Day 310 or November 6) dates of the rainy season are indicated in the figure.

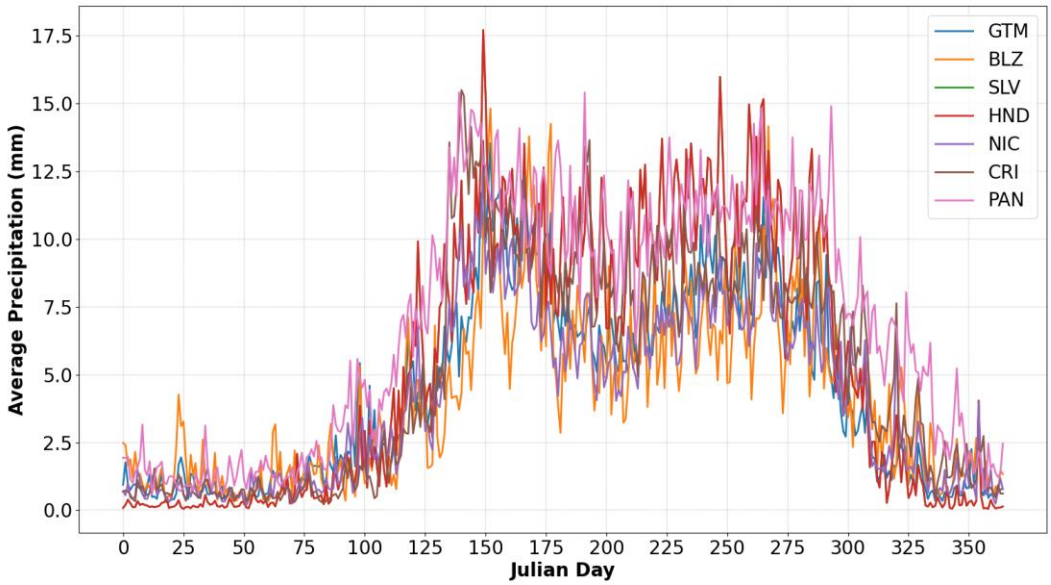

Figure S2: The 22-year (2001-2022) daily climatological rainfall which is area averaged to depict the seasonality of the rainfall over Guatemala (GTM), Belize (BLZ), El Salvador (SLV), Honduras (HND), Nicaragua (NIC), Costa Rica (CRI), Panama (PAN) from the 12-h latency IMERG product.

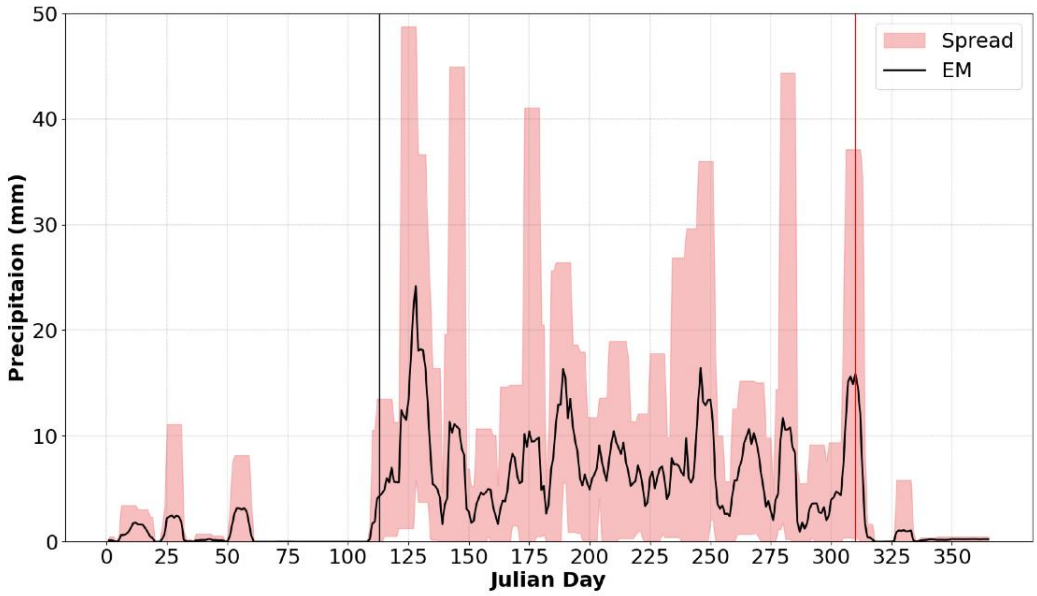

Figure S3: The Ensemble Mean (EM) of 1001 members (solid black line) of daily timeseries of precipitation over a specific grid point over Nicaragua with the corresponding range of values from the ensemble (spread) shown in the red shade for the year 2009. The median start and retreat dates of the wet season for 2009 for this grid point are shown by the vertical, solid black and red lines, respectively.

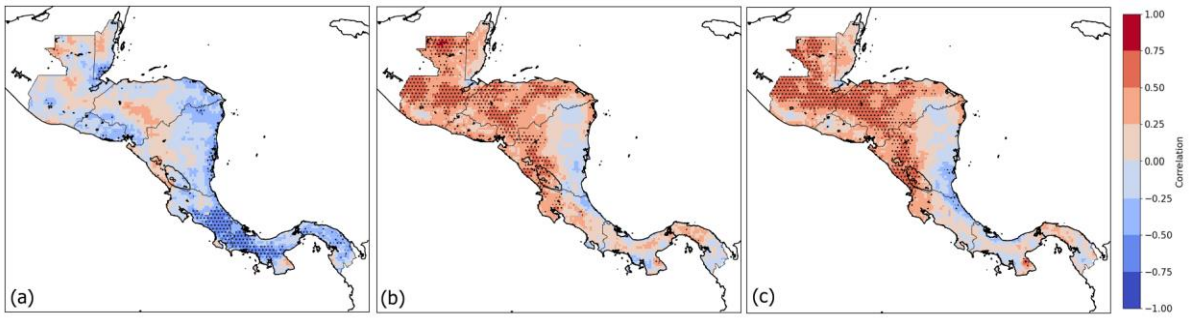

Figure S4: The correlation of anomalies seasonal rain with a) the Atlantic Warm Pool area index (Misra et al. 2014) and tropical north Atlantic SST in b) April and c) July. The seasonal mean Atlantic Warm Pool area index was computed from its onset to demise date, which is approximately from July to October. The statistically significant values at a 5% significance level according to the t-test are stippled. Field significance at the 95% confidence level following Livezey and Chen (1983) is verified.